JVI Journals.ASM.org

Functional Analysis of the Murine Coronavirus Genomic RNA Packaging Signal

Lili Kuo, Paul S. Masters

Wadsworth Center, New York State Department of Health, Albany, New York, USA

Coronaviruses selectively package genomic RNA into assembled virions, despite the great molar excess of subgenomic RNA species that is present in infected cells. The genomic packaging signal (PS) for the coronavirus mouse hepatitis virus (MHV) was originally identified as an element that conferred packaging capability to defective interfering RNAs. The MHV PS is an RNA structure that maps to the region of the replicase gene encoding the nonstructural protein 15 subunit of the viral replicase-transcriptase complex. To begin to understand the role and mechanism of action of the MHV PS in its native genomic locus, we constructed viral mutants in which this *cis*-acting element was altered, deleted, or transposed. Our results demonstrated that the PS is pivotal in the selection of viral genomic RNA for incorporation into virions. Mutants in which PS RNA secondary structure was disrupted or entirely ablated packaged large quantities of subgenomic RNAs, in addition to genomic RNA. Moreover, the PS retained its function when displaced to an ectopic site in the genome. Surprisingly, the PS was not essential for MHV viability, nor did its elimination have a severe effect on viral growth. However, the PS was found to provide a distinct selective advantage to MHV. Viruses containing the PS readily outcompeted their otherwise isogenic counterparts lacking the PS.

Virion assembly culminates in the packaging of viral genetic material in a protected form that can be transmitted to a new host. Many viruses exhibit a marked preference for packaging their own genomes, to the exclusion of other available nucleic acids, but the molecular basis for this preference is understood in only a few cases. Coronaviruses are very large RNA viruses with an elaborate mechanism of gene expression that entails the synthesis of a 3′-nested set of subgenomic mRNAs (sgRNAs) (1, 2). Each sgRNA contains a leader segment, which is identical to the 5′ end of the genome, joined at a downstream transcription-regulating sequence (TRS) to a segment identical to the 3′ end of the genome. Despite the multiplicity of full-length and sgRNA species of both polarities that come into play during the course of intracellular replication, it is generally agreed that coronaviruses selectively package positive-strand genomic RNA (gRNA) into virions. Purified virions of mouse hepatitis virus (MHV) and transmissible gastroenteritis virus (TGEV) have been shown to almost exclusively contain gRNA (3–6), but it is not well established whether this high degree of selectivity is shared by all members of the coronavirus family (7, 8).

In MHV, the genomic packaging signal (PS) was localized through comparative analysis of packaged and unpackaged defective interfering (DI) RNAs (3, 4). DI RNAs are variants of gRNA that contain multiple extensive deletions and therefore can propagate only by parasitizing the replicative machinery of a helper virus. The exact functional boundaries of the MHV PS are not precisely defined, but different studies have converged on a 220-nucleotide region that is centered some 20.3 kb from the 5′ end of the genome (5, 9, 10). This situates the PS in rep 1b, the downstream portion of the gene for the viral replicase-transcriptase complex (Fig. 1). Such a location would ensure that the PS appears only in gRNA and not in any of the sgRNAs. The product of the replicase gene is a huge polyprotein that is autoproteolytically processed into 16 nonstructural proteins. The PS is embedded in the coding sequence for nonstructural protein 15 (nsp15), a hexameric uridylate-specific endoribonuclease (11–13).

Although early work suggested a 69-nucleotide RNA secondary structure as the minimal functional MHV PS (5, 14), larger forms of the element were shown to be required for optimal efficiency (10, 15, 16). A folding for one larger version of the PS was predicted but was not experimentally verified (15). Recently, a novel structural model for the MHV PS was proposed by the Olsthoorn laboratory (17). This new structure, a 95-nt bulged stem-loop, was strongly supported by chemical and enzymatic probing experiments. It was also found to be highly conserved among lineage A betacoronaviruses, a subgenus that includes human coronavirus HKU1 (HCoV-HKU1), as well as bovine coronavirus (BCoV), human coronavirus OC43, and related viruses within the betacoronavirus 1 species (18). This phylogenetic conservation is consistent with the earlier demonstration that the BCoV PS is functionally interchangeable with its MHV counterpart (15). However, the structural and functional homology of the PS does not extend to other lineages within the betacoronaviruses or to other genera. It is clear, for example, that there is not a counterpart of the MHV PS in the nsp15 open reading frame (ORF) of the lineage B betacoronavirus severe acute respiratory syndrome coronavirus (SARS-CoV), the alphacoronavirus TGEV, or the gammacoronavirus infectious bronchitis virus (IBV) (19, 20). Moreover, studies characterizing packaged DI RNAs of TGEV and IBV suggest that the packaging signals for these viruses map to distant sites (6, 21).

We have begun to genetically manipulate the MHV PS with the goal of identifying its interacting partners and defining the mechanism of packaging. Although the PS was discovered by use of DI RNA systems, the role of this element in its native locus in gRNA has never been tested. Our study found that the PS does govern the

Received 11 January 2013 **Accepted** 15 February 2013
Published ahead of print 28 February 2013
Address correspondence to Paul S. Masters, masters@wadsworth.org.

doi:10.1128/JVI.00100-13

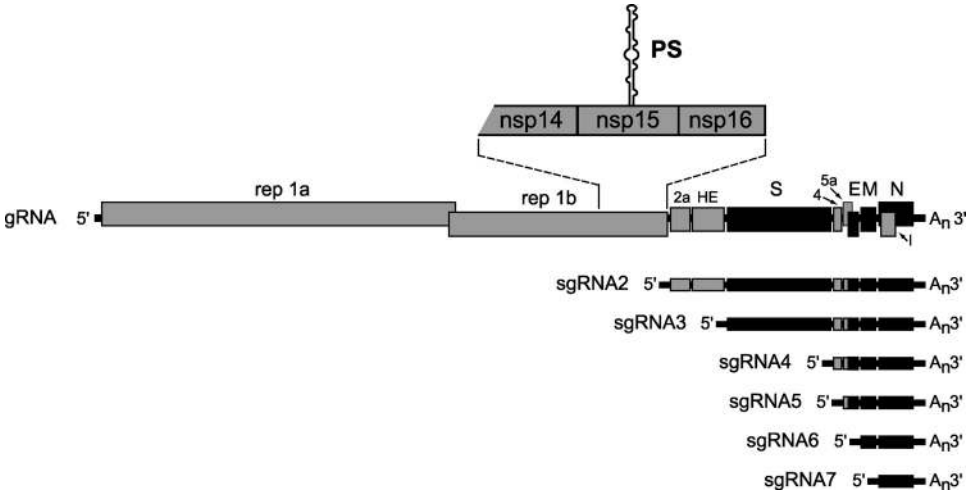

FIG 1 MHV RNA species. The 31.3-kb MHV genome (gRNA) is shown with an expanded segment detailing the 3′ terminus of the replicase gene (rep 1a and 1b), including the region encoding nsp14 to nsp16. The position of the packaging signal (PS) within the coding region for nsp15 is indicated. Downstream of the replicase gene are the genes for structural proteins (spike [S], envelope [E], membrane [M], and nucleocapsid [N]) and for accessory proteins (2a, hemagglutinin-esterase [HE], 4, 5a, and internal [I]). Beneath the gRNA is the 3′-nested set of transcribed subgenomic RNA (sgRNA) species that is a defining characteristic of coronaviruses and other members of the order *Nidovirales*.

selective incorporation of gRNA into virions, and it remains functional when transposed to an ectopic genomic site. Remarkably, however, the PS is not essential for MHV viability, but it confers a selective advantage to genomes that harbor it.

MATERIALS AND METHODS

Cells and viruses. The MHV-A59 wild type and all mutants were grown in mouse 17 clone 1 (17Cl1) cells. Plaque titrations and plaque purifications were performed with mouse L2 cells. The interspecies chimeric virus designated fMHV.v2 (22), which was used for mutant construction, was grown in FCWF (*Felis catus* whole fetus) cells.

MHV mutant construction. All mutants in this study were constructed by targeted RNA recombination, as described in detail previously (22, 23). In brief, feline cells were infected with fMHV.v2, which bears the ectodomain of the feline coronavirus spike (S) protein, and were then transfected with synthetic donor RNA containing the mutations to be incorporated. Progeny virus that reacquired the MHV S gene were selected, based on restoration of the ability to grow in murine cells, and mutants were subsequently identified through screening by reverse transcription-PCR (RT-PCR).

The wild-type parent transcription vector for synthesis of donor RNA was pPM9 (Fig. 2), which was constructed, in multiple steps, from the previously described pMH54 (23). Vector pPM9 contains 5′ elements of the MHV-A59 genome linked to the 3′ end of the genome, the latter starting from codon 236 of nsp14. Two alterations were made in pPM9 with respect to the authentic wild-type sequence. First, two unique coding-silent restriction sites were created to flank the region of the PS. An XbaI site (underlined) was generated by changing codons 124 to 126 of nsp15 from GCTCTTGAA to GCTCTAGAA, and a BspEI site (underlined) was produced by changing codons 313 to 314 of nsp15 from AG TGGT to TCCGGA. Second, a 2,079-bp deletion was created downstream of the nsp16 stop codon, removing transcription-regulating sequence 2 (TRS2), gene 2a, and all except 99 bp of the hemagglutinin-esterase (HE) gene. A 31-bp linker containing unique SalI and AscI sites was inserted in place of the deleted region (24). Downstream of the start of the S gene, other engineered sequence differences carrying over from pMH54 to pPM9 have been noted previously (23).

Transcription vectors for the silPS mutant (pPM17; a mutant in which 20 coding-silent mutations were created in the interval of the nsp15 ORF containing this element) and the ΔPS mutant (pPM22; a mutant containing a packaging element deletion) were constructed from pPM9 by replacement of the XbaI-BspEI segment with a fragment synthesized either from overlapping oligonucleotides by PCR or else by two-step PCR. Transcription vectors for the silPS-PS2 mutant (pPM20) and the ΔPS-PS2 mutant (pPM19) were constructed by insertion of a PCR product containing bp 514 to 681 of nsp15 in place of the SalI-AscI fragment of pPM17 or pPM22, respectively.

Virus purification. Purifications of wild-type and mutant viruses by ultracentrifugation in glycerol-tartrate gradients (25) or in sucrose gradients (4, 5) were carried out as described previously. For immunopurifications, we employed a modification of the procedure of Escors et al. (6). Virus was grown in 12 T150 flasks of 17Cl1 cell monolayers in Eagle's

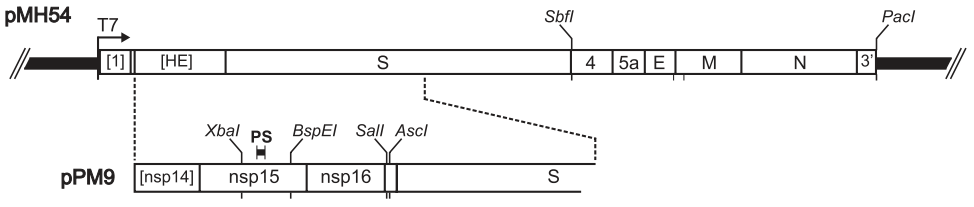

FIG 2 Donor RNA transcription vector for construction of MHV PS mutants by targeted RNA recombination (22, 23). All mutants in the current work originated with the parent vector pPM9, which was derived from the previously described pMH54 (23) by the addition of genomic cDNA upstream of the S gene. The locus containing the PS is indicated by a bar above nsp15. Shown are coding-silent unique XbaI and BspEI sites flanking the PS and unique SalI and AscI sites in the truncated nonessential intergenic region between nsp16 and the S gene.

medium containing 10% fetal bovine serum. Following polyethylene glycol precipitation from growth medium, virions were resuspended in magnesium- and calcium-free phosphate-buffered saline, pH 7.4 (PBS), and were pelleted onto cushions of 60% sucrose in PBS by centrifugation for 2 h at 151,000 × *g* in a Beckman SW41 rotor at 4°C. An aliquot equivalent to one-sixteenth of the collected virions was incubated with 1 ml of anti-M monoclonal antibody J.1.3 for 3 h at 4°C and then for an additional 3 h with 1 ml of a 75% slurry of nProtein A Sepharose (GE Healthcare) in PBS. Sepharose beads were collected by centrifugation at 200 × *g* for 10 min at 4°C, washed three times with 10 ml PBS, and used directly for RNA purification or SDS-PAGE sample preparation.

Analysis of viral RNA. RNA was extracted from purified virions or from infected cell monolayers with Ultraspec reagent (Biotecx) per the manufacturer's instructions or by using Direct-zol RNA miniprep spin columns (Zymo Research). For verification of constructed mutants and for analysis of competition experiments, reverse transcription of isolated RNA was conducted with a random hexanucleotide primer and avian myeloblastosis virus reverse transcriptase (Life Sciences). PCR amplification of cDNA was performed with the Expand high-fidelity PCR system (Roche). RT-PCR products were analyzed by agarose gel electrophoresis or were purified with QIAquick spin columns (Qiagen) prior to DNA sequencing. Northern blotting of purified virion RNA was carried out as detailed previously (24). RNA was probed with a PCR product corresponding to the 3′-most 539 nucleotides of the N ORF and the entire 3′ untranslated region of the MHV genome, which was labeled with an AlkPhos Direct kit and was visualized using the CDP-Star detection reagent (GE Healthcare).

Protein analysis. Western blotting of purified virions or of NP-40 lysates prepared from infected 17Cl1 cell monolayers was carried out exactly as described previously (26). Prestained protein standards (SeeBlue Plus2; Invitrogen) were included in adjacent lanes in SDS-PAGE. Proteins were detected with anti-N monoclonal antibody J.3.3 and anti-M monoclonal antibody J.1.3 (both generously provided by John Fleming, University of Wisconsin, Madison, WI). Bound antibodies were visualized by enhanced chemiluminescence detection (Pierce), which was quantitated with a Bio-Rad ChemiDoc XRS+ instrument.

Virus growth and competition assays. The growth kinetics of mutant and wild-type viruses were measured in infections begun at multiplicities of 0.01 or 5.0 PFU per cell exactly as described previously (27). To assay the relative fitness of the ΔPS mutant and its wild-type counterpart, 10-cm^2 wells of 17Cl1 cells were infected with a mixture of both viruses at a constant multiplicity of 1 PFU per cell of the silPS virus and multiplicities of either 1, 0.1, or 0.01 PFU per cell of the wild type. At 12 h postinfection, when monolayers exhibited maximal syncytium formation but little detachment, released virus was harvested, and RNA was purified from the monolayer. Harvested virus (300 μl of 4 ml total) was used to infect a fresh set of monolayers, and the process was repeated for a total of five passages. The silPS and silPS-PS2 mutant pair were assayed in the same manner. The composition of purified infected cell RNA was monitored by RT-PCR. The primers for analysis of the native PS locus were PM166 (nsp15 nucleotides 352 to 369) and PM406 (complementary to nsp15 nucleotides 920 to 952); the primers for analysis of the PS2 marker were CM6 (nsp16 nucleotides 634 to 651) and CM31 (complementary to nucleotides 65 to 82 upstream of the S gene).

RESULTS

Construction of an MHV mutant with a disrupted PS. The structure proposed by the Olsthoorn laboratory (17) for the PS of lineage A betacoronaviruses is a 95-nt bulged stem-loop, which, for MHV, encompasses bases 20,273 to 20,367 of the genome (Fig. 3A). This element contains four copies of an AGC/GUAAU motif repeated at regular intervals, each copy of which displays an AA or GA bulge on its 3′ side. An internal loop, which varies among different viruses, divides the PS into two quasisymmetric halves.

To test the functional significance of the MHV PS, we constructed a mutant, designated silPS, in which 20 coding-silent mutations were created in the interval of the nsp15 ORF containing this element (Fig. 3B). Changes were chosen to generate only codons of equivalent or greater codon usage frequency for the mouse (28) (http://www.kazusa.or.jp/codon/). Collectively, these mutations widely altered the primary sequence and completely abolished the RNA secondary structure of the PS. None of the three structures for silPS predicted by Mfold (29), one of which is shown in Fig. 3B, contained any apparent vestige of the features of the PS. It should be noted that the 20 mutations also disrupted alternative proposed structures for the PS (5, 15). Additionally, in both the silPS mutant and its corresponding wild-type counterpart, the nonessential genes 2a and HE were deleted, and their associated TRS (TRS2) was knocked out (Fig. 3D). The net effect of these latter alterations was the creation of a region of 128 nucleotides downstream of the replicase gene that is unique to gRNA and is not transcribed into any of the sgRNAs. The deletion of the 2a and HE genes of MHV has been shown to have no effect on growth of the virus in tissue culture (30–32).

The silPS mutant and its isogenic wild-type control virus were constructed by targeted recombination of synthetic donor RNAs with the interspecies chimeric coronavirus fMHV (22, 23). This method of coronavirus reverse genetics relies on selection for the reacquisition of the MHV S gene. However, because all of the mutations of interest in this case fell upstream of the S gene, silPS and wild-type recombinants were subsequently identified through screening. Two independent silPS mutants, designated Alb650 and Alb651, were isolated. Since both behaved identically in preliminary experiments, one of them (Alb651) was chosen for further analysis in comparisons with an isogenic wild-type recombinant, Alb649.

Phenotype of the silPS mutant. Our initial expectation had been that disruption of the PS would be severely debilitating, if not lethal, for the virus. We were therefore surprised to find that the silPS mutant formed plaques that were indistinguishable in size from those of the wild type at 33, 37, and 39°C (Fig. 4A). Moreover, there was little detectable difference between the growth kinetics of the silPS mutant and those of the wild type, either in multicycle, low-multiplicity infections (Fig. 4B) or in single-step, high-multiplicity infections (Fig. 4C). A second, independent growth comparison gave results identical to those in Fig. 4B and C. One reproducibly observed dissimilarity was that in low-multiplicity infections, after reaching a peak at 30 h postinfection, titers of the silPS mutant dropped some 0.5 to 1 $\log_{10}$ relative to those of the wild type by 48 h postinfection. Also, in these experiments and in infections for preparative purposes it was consistently noted that the silPS mutant, despite producing widespread syncytia, never caused as extensive a cytopathic effect and detachment of the cell monolayer as did the wild type. (The same was true for the subsequently isolated ΔPS mutant.) We do not yet know the basis for these observations.

To determine the effect of the silPS mutations on packaging, we analyzed the RNA and protein content of extensively purified virions. In preliminary experiments, we prepared virions by two rounds of centrifugation in either glycerol-tartrate gradients (25) or sucrose gradients (4, 5); alternatively, virions were isolated by immunopurification (6). In agreement with the findings of Escors and coworkers with TGEV (6), we observed the highest stringency of packaging, i.e., the least incorporation of sgRNAs, in wild-type virions that were immunopurified (data not shown). Conse-

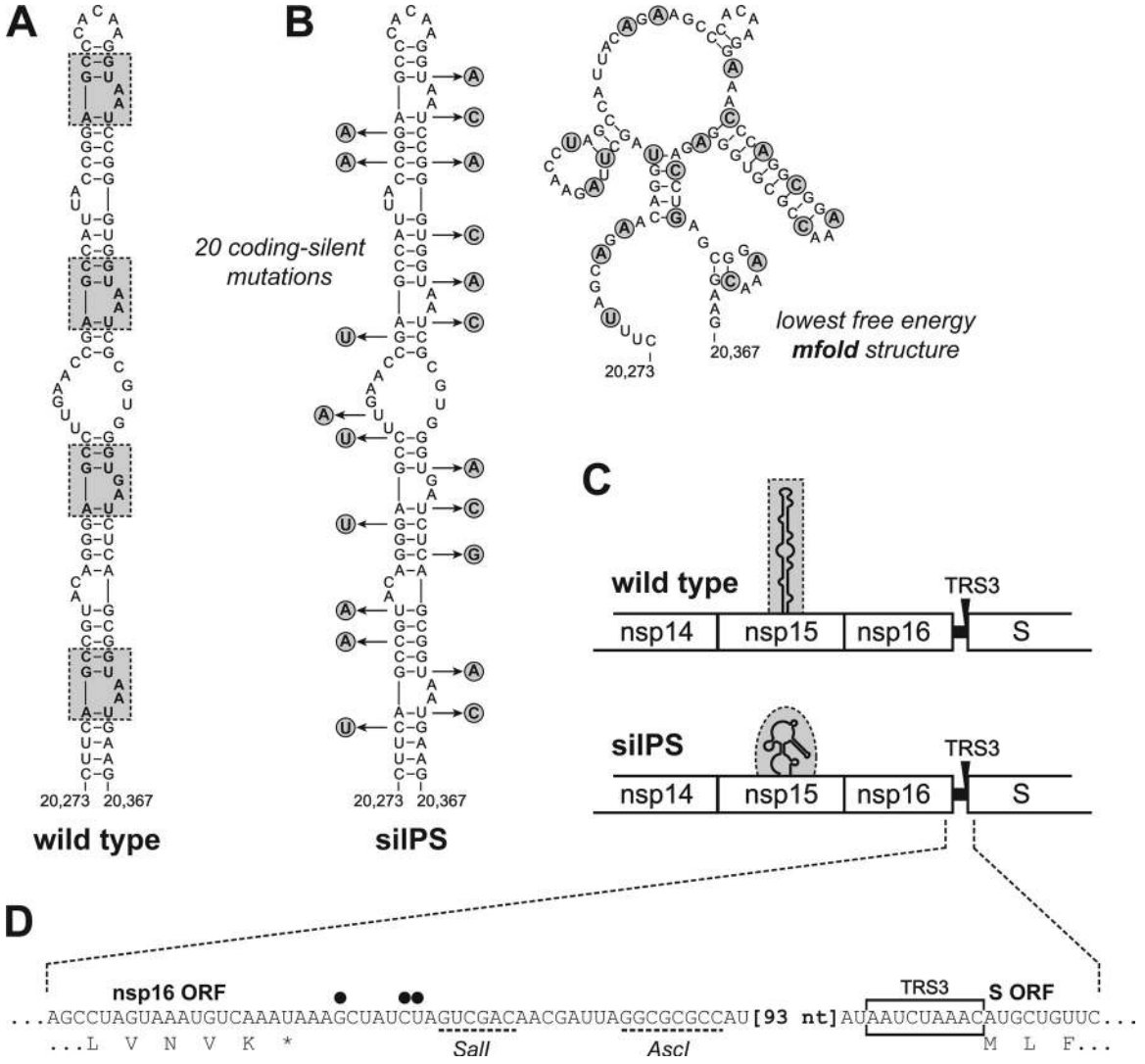

FIG 3 Construction of the silPS mutant. (A) Model for the MHV PS proposed by Chen et al. (17). The four repeating units with AA (or GA) bulges are boxed. (B) Positions and identities of 20 mutations (circled nucleotides) made to disrupt the structure of the PS without altering the encoded amino acid sequence of nsp15. The resulting lowest-free-energy structure predicted by Mfold (29) for the mutated sequence is shown on the right. (C) Schematics of the relevant genomic regions of the constructed silPS mutant and its isogenic wild-type counterpart. (D) Detail of the region downstream of the replicase gene, in which TRS2 was knocked out, all of gene 2a was deleted, and all except 99 nucleotides of the HE gene was deleted. The positions of SalI and AscI sites created in the parent transcription vector pPM9 are shown. Circles above the sequence indicate nucleotides that were mutated to knock out TRS2.

quently, this procedure was adopted for the remainder of the present study. The silPS mutant and wild-type virus were grown, titrated by plaque assay, and immunopurified with a monoclonal antibody specific for the ectodomain of the M protein, as outlined in Fig. 5A and described in detail in Materials and Methods. Following quantitation of virions by Western blotting for N protein, the protein compositions of equal amounts of silPS and wild-type virions were examined by Western blots probed with monoclonal antibodies specific for the N and M proteins (Fig. 5B) and by Coomassie blue staining of virions separated by SDS-polyacrylamide gel electrophoresis (Fig. 5C). This showed that there were no differences between the mutant and the wild type in either the profiles or the ratios of virion structural proteins that they each contained, nor did either exhibit obvious incorporation of nonviral proteins. Thus, disruption of the PS did not appear to cause any gross aberrations in viral protein assembly.

Northern blot analysis of RNA from the cells in which virus had been grown demonstrated the presence of the expected set of gRNA and sgRNAs for both the silPS mutant and its wild-type counterpart (Fig. 5D). Owing to the 3′-nested set structure of coronavirus RNAs (Fig. 1), all species were detected with a probe specific for the 3′ end of the genome, and because of the knockout of TRS2, sgRNA2 was not synthesized. In contrast to the pattern of intracellular viral RNA, RNA isolated from purified wild-type virions was almost entirely devoid of sgRNA (Fig. 5E), consistent with previous work showing a high degree of selective packaging of gRNA by MHV (3–5). Virions of the silPS mutant, however, were seen to have packaged substantial amounts of sgRNAs, and these were present in direct proportion to their relative intracellular abundance. These results established that the PS, in its native genomic locus, does indeed govern the selectivity of viral gRNA packaging.

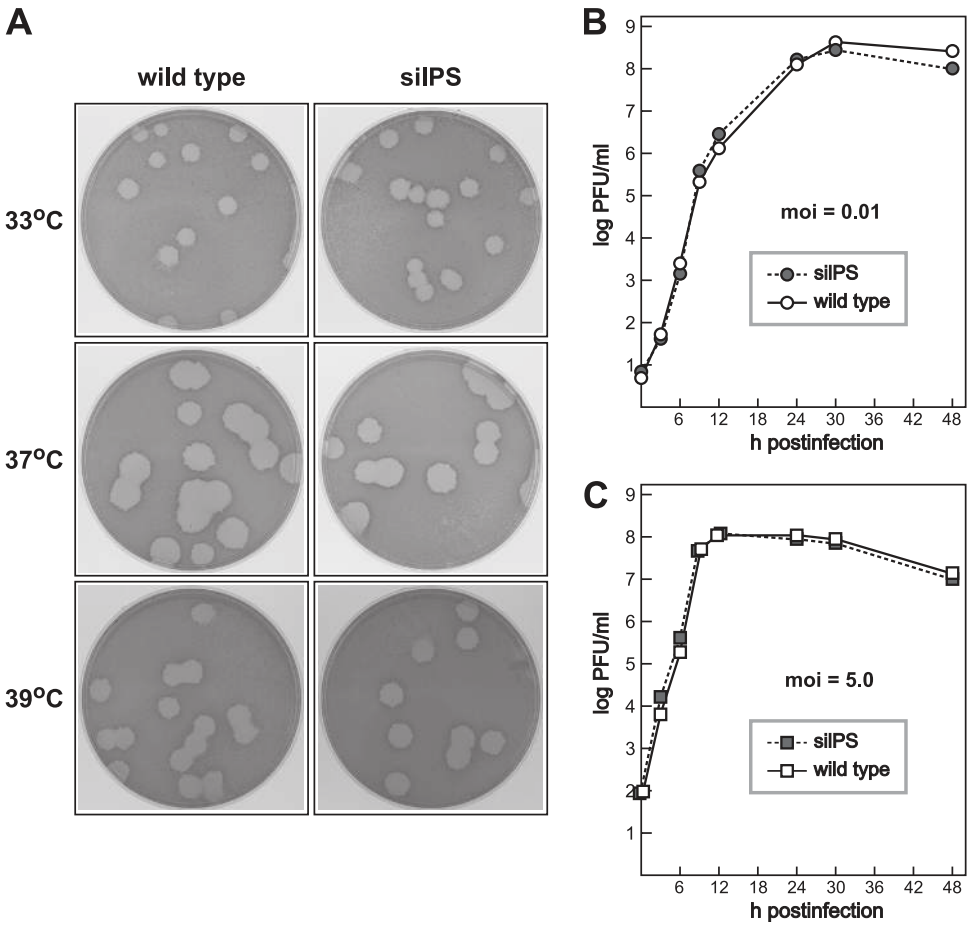

FIG 4 Growth characteristics of the silPS mutant. (A) Plaques of the silPS mutant at 33, 37, and 39°C compared with those of the isogenic wild-type virus. Plaque titrations were carried out on L2 cells; monolayers were stained with neutral red at 72 h postinfection and were photographed 18 h later. (B and C) Growth kinetics of the silPS mutant relative to the wild type. Confluent monolayers of 17Cl1 cells were infected at the indicated multiplicity of infection (moi). At the indicated times postinfection, aliquots of medium were removed, and infectious titers were determined by plaque assay on L2 cells.

Construction and characterization of mutants in which the PS was deleted or transposed to a different genomic site. It still remained possible that the silPS mutations failed to abolish all essential features of the PS. To learn if the silPS mutant represented the null phenotype for packaging we next sought to entirely delete the PS from the MHV genome. Although the MHV PS falls within the ORF for nsp15, a critical component of the viral replicase-transcriptase complex, the PS encodes a surface loop joining the amino- and carboxy-terminal domains of the mature nsp15 molecule (Fig. 6A). This localization was first noted in a comparison of the MHV and SARS-CoV nsp15 structures (19). A portion of the MHV nsp15 loop is presumed to be flexible, as it is missing from the crystal structure (33); moreover, the loop falls on the outward-facing surface of each unit in the nsp15 hexamer. Accordingly, we designed a packaging element deletion (ΔPS) based on an alignment of nsp15 sequences of lineage A betacoronaviruses with those of other coronaviruses that lack this PS (Fig. 6B). In the ΔPS mutant, nsp15 amino acids F184 through E214 were removed and replaced with a heterologous pentapeptide sequence, NGNGN. At the RNA level, the corresponding short substitution (AACGGCAATGGCAAC) is predicted by Mfold to be completely unstructured (Fig. 6C). The ΔPS mutant was also engineered to contain the abbreviated intergenic region downstream of the replicase gene that was made in the silPS mutant (Fig. 6D). As an adjunct, we constructed a related mutant, ΔPS-PS2, in which the PS was deleted from its original position and inserted ectopically in the intergenic region, at a position that was 15 nucleotides downstream of the replicase gene stop codon and 105 nucleotides upstream of TRS3. This move placed the center of the PS 1,525 nucleotides from its original position. The PS2 insertion comprised the structure shown in Fig. 6C plus 35 and 38 nucleotides, respectively, of its 5′ and 3′ flanking regions from the nsp15 ORF.

For each mutant, two independent isolates were obtained by targeted RNA recombination and screening (Alb743 and Alb746 for ΔPS, Alb758 and Alb760 for ΔPS-PS2). Data are presented for one set (Alb746 and Alb760), but both independent isolates of each mutant behaved identically. As we had seen with the silPS mutant, the ΔPS mutant formed plaques at 33, 37, and 39°C that were equal in size to those of its wild-type and ΔPS-PS2 counterparts (Fig. 7A). The ΔPS virus also grew to high titers comparable to those of the wild type. Thus, the virus was not significantly impaired by loss of either the PS or the nsp15 peptide linker that it encodes. Northern blot analysis of immunopurified virions showed that, to the same extent as the silPS mutant, the ΔPS mutant packaged large amounts of sgRNAs (Fig. 7B). Side-by-side

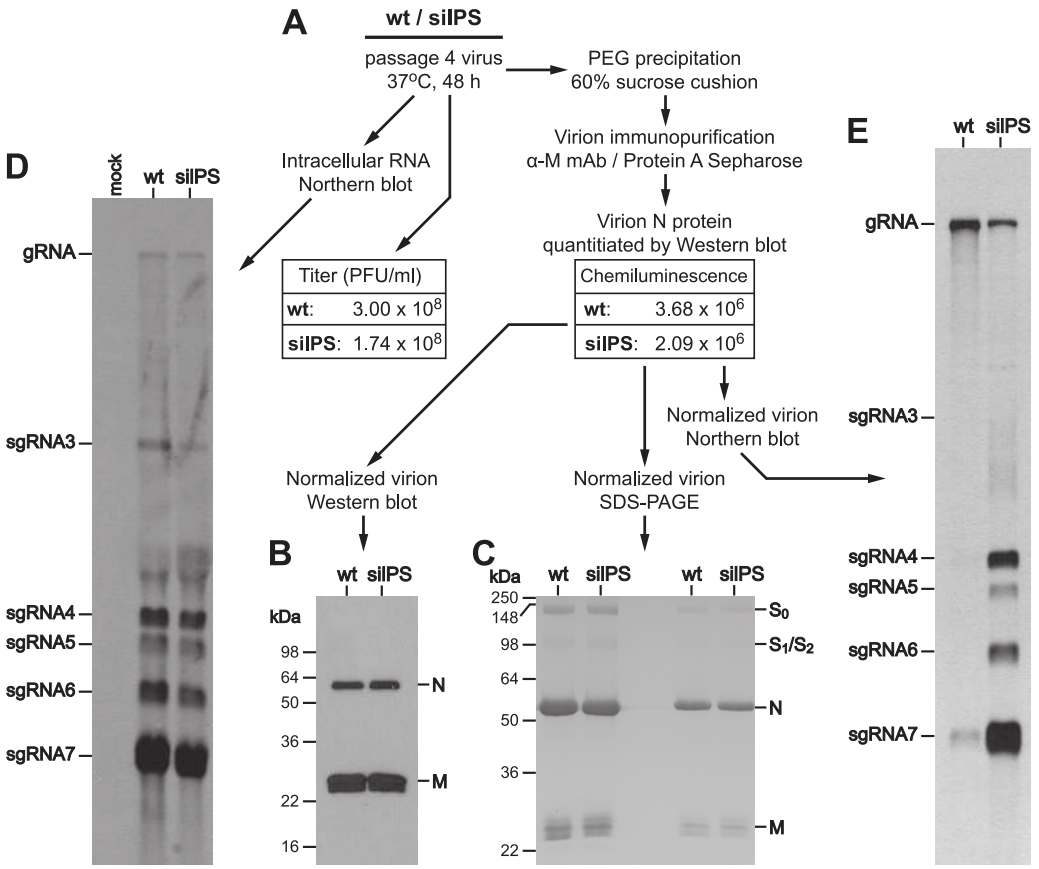

FIG 5 RNA packaging phenotype of the silPS mutant. (A) Outline of the procedures for purification, normalization, and analysis of silPS and wild-type virions, as detailed in Materials and Methods. Infectious titers were determined by plaque assay on L2 cells at 37°C; chemiluminescence values are given in arbitrary volume units, as measured with a Bio-Rad ChemiDoc XRS+ instrument. (B) Western blot of normalized amounts of immunopurified wild-type and silPS virions probed with anti-N monoclonal antibody J.3.3 and anti-M monoclonal antibody J.1.3. (C) Coomassie blue-stained SDS-polyacrylamide gel of normalized amounts of immunopurified wild-type and silPS virions; samples on the right are a 5-fold dilution of those on the left. Molecular mass standards are indicated on the left of each panel (B and C). (D) Northern blot of total RNA isolated from infected 17Cl1 cells, from which wild-type or silPS virions were purified, or from mock-infected cells. (E) Northern blot of RNA isolated from normalized amounts of immunopurified wild-type and silPS virions. MHV RNA was detected with a probe specific for the 3′ end of the genome (D and E).

Northern blots of the silPS and ΔPS mutants were indistinguishable (data not shown), which indicated that the ΔPS mutant was not more extensively defective in RNA packaging selectivity than the silPS mutant. In contrast, the ΔPS-PS2 mutant exhibited the same degree of gRNA packaging selectivity as did the wild type (Fig. 7B). This result established that the PS, with a minimal amount of flanking sequence, is sufficient to impart packaging selectivity, and it can operate at a genomic site other than its native locus in the replicase gene. Additionally, the phenotype of the ΔPS-PS2 mutant showed that the functionality of the PS is not coupled to translation of the region in which it resides.

Fitness advantage provided by the PS. Although our results clearly demonstrated a discriminating role for the PS in virion particle assembly, we had not observed a measurable impact of that role on virus growth. To further probe whether the MHV PS provides any detectable benefit to viruses that harbor it, we carried out competition assays. In the initial set of experiments, monolayers of cells were infected with mixtures of the ΔPS mutant and the wild type, and progeny viruses were serially propagated for a total of five passages. The input virus for the first passage consisted of equal numbers of PFU of each virus, or else it was weighted 10:1 or 100:1 in favor of the ΔPS mutant. Following each passage, infected-cell RNA was isolated and analyzed by RT-PCR using primers in the nsp15 ORF that would monitor the presence or absence of the PS. It should be noted that the same primer pair was used to detect RNA from both viruses. Thus, if there had been any bias in the PCR, it would have been expected to favor the smaller amplicon (that of the ΔPS mutant). In all cases, a strong advantage for the wild-type virus was obvious (Fig. 8A). At PFU input ratios of 1:1 or 10:1, the wild type was seen to predominate as early as the first or second passage and the ΔPS mutant was no longer detectable by the third or fourth passage. Even at a PFU input ratio of 100:1, the wild type decisively overtook the ΔPS mutant by the fourth passage. An independent duplicate of the experiment shown in Fig. 8A yielded the same results. This outcome implied that, in growth in tissue culture, a virus containing the PS was rapidly selected over one that lacked the PS.

We could not completely rule out, however, the possibility that the deletion in the ΔPS mutant exerted some deleterious effect on nsp15. It has been shown previously that particular mutations constructed in the carboxy-terminal domain of MHV nsp15 can alter viral phenotype (13, 34). That this was not the case for the

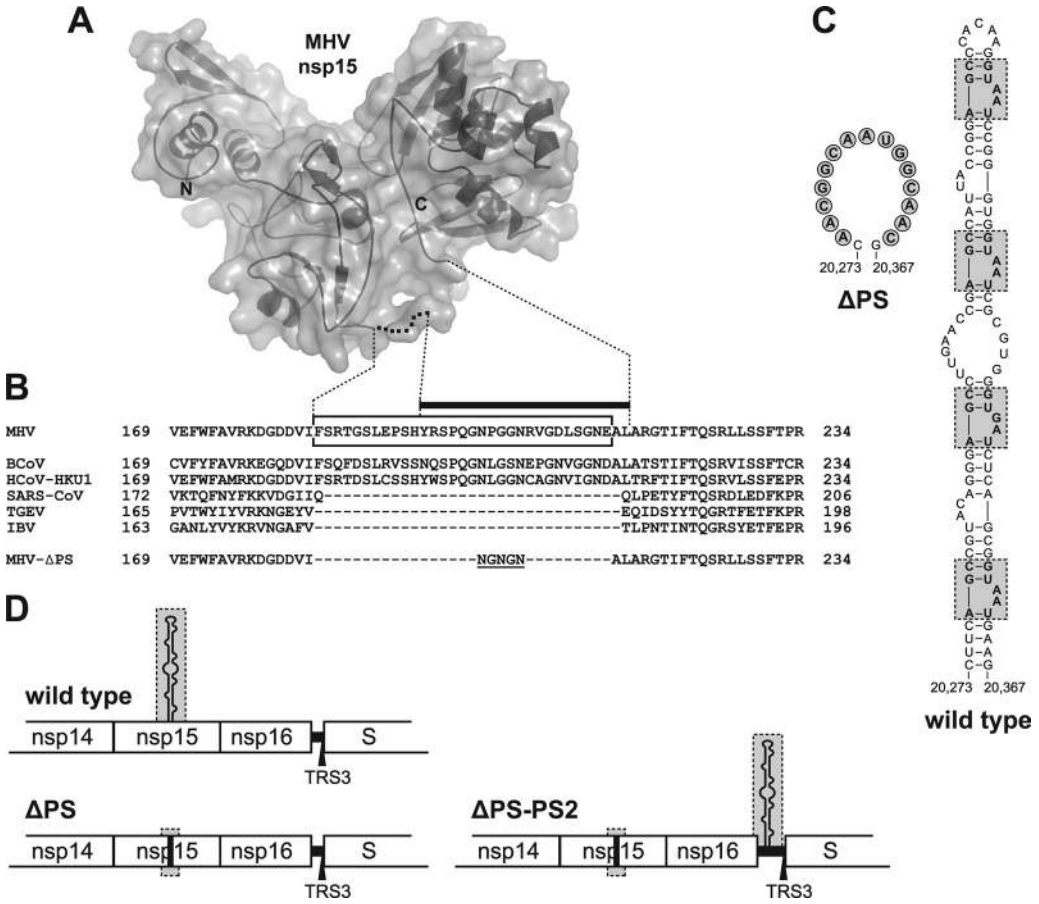

FIG 6 Construction of the ΔPS and ΔPS-PS2 mutants. (A) Ribbon diagram and molecular surface rendering of the MHV nsp15 monomer (PDB accession code 2GTH) (33) generated with PyMol (http://pymol.org). The nsp15 amino and carboxy termini are labeled N and C, respectively. The dotted line represents part of the surface loop connecting the amino- and carboxy-terminal domains of the protein. (B) Alignment of the central region of nsp15 of MHV with that of representative coronaviruses: lineage A betacoronaviruses BCoV and HCoV-HKU1, lineage B betacoronavirus SARS-CoV, alphacoronavirus TGEV, and gammacoronavirus IBV. GenBank accession numbers for the sequences shown are as follows: MHV, AY700211; BCoV, U00735; HCoV-HKU1, AY597011; SARS-CoV, AY278741; TGEV, AJ271965; and IBV, AJ311317. Boxed residues in the MHV sequence are those that are encoded by the PS and that were deleted in the ΔPS mutant. The bar above the alignment indicates flexible loop residues (Y195 through L216) that are missing from the crystal structure of MHV nsp15 (33). Dotted lines connect deleted and missing residues to their corresponding positions in the structure in panel A. At the bottom of the alignment, the five heterologous amino acids encoded by the substituted sequence in the ΔPS mutant are underlined. (C) Representation of the unstructured 15-nt sequence substituted for the PS in the ΔPS mutant compared to the wild-type PS. (D) Schematics of the relevant genomic regions of the constructed ΔPS mutant, the ΔPS-PS2 mutant, and their isogenic wild-type counterpart.

ΔPS mutant was suggested by experiments in which the ΔPS and the silPS mutants competed, which did not reveal a dominance of one virus over the other. To resolve this uncertainty, we performed an experiment involving competition between the silPS virus and a silPS-PS2 mutant (Alb767), the latter of which had been constructed in a manner entirely analogous to the ΔPS-PS2 mutant (Fig. 8B). Thus, the two competing viruses contained the same coding-silent disruption of the PS in the nsp15 ORF and differed only in the presence or absence of a copy of the PS in the intergenic region downstream of the replicase gene. As with the initial competition assay, the input inoculum for the first passage contained equal PFU of each virus, or else it was weighted 10:1 or 100:1 in favor of the silPS mutant. In this case, RT-PCR analysis was carried out with a primer pair chosen to amplify the intergenic region between the replicase and S genes. For a PFU input ratio of 1:1, we observed that the silPS-PS2 virus overtook the silPS virus by the second or third passage. (An RT-PCR product of intermediate mobility [Fig. 8B] was shown by both sequencing and further PCR analysis to be a heteroduplex composed of opposite strands of the silPS and silPS-PS2 products.) The predominance of the silPS-PS2 virus was delayed only until the third or fourth passage, when the PFU input ratio was increased to 10:1. Even at the highly skewed input ratio of 100:1, where the silPS-PS2 mutant was barely detectable at the first passage, it was seen to be increasing disproportionately by the fourth and fifth passages, indicating that it was outcompeting the silPS mutant. The same outcome was obtained in an independent repeat of the experiment shown in Fig. 8B. These results, although not as dramatic as those obtained with the ΔPS mutant, confirmed that the presence of the PS affords a definite fitness advantage to MHV.

DISCUSSION

The MHV PS was originally defined as an element that enabled DI RNAs to be packaged in the presence of coreplicating helper virus (3, 4), but the *in situ* role of the PS in the MHV genome has until now remained unexplored. We approached this question by iso-

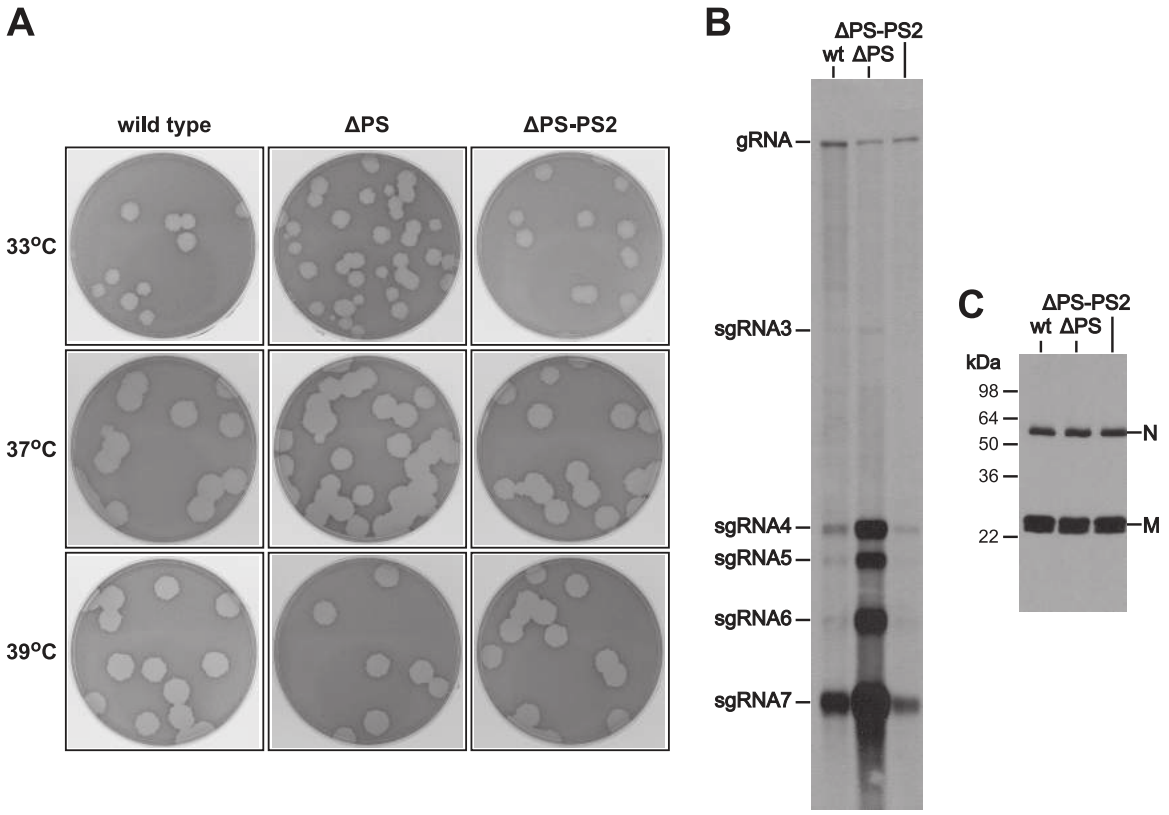

FIG 7 Growth and RNA packaging by the ΔPS and ΔPS-PS2 mutants. (A) Plaques of the ΔPS and ΔPS-PS2 mutants at 33, 37, and 39°C compared with those of the isogenic wild-type virus. Plaque titrations were carried out on L2 cells; monolayers were stained with neutral red at 72 h postinfection and were photographed 18 h later. (B) Northern blot of RNA isolated from normalized amounts of immunopurified wild-type, ΔPS, and ΔPS-PS2 virions detected with a probe specific for the 3′ end of the genome. (C) Western blot of normalized amounts of immunopurified wild-type, ΔPS, and ΔPS-PS2 virions probed with monoclonal anti-N antibody J.3.3 and monoclonal anti-M antibody J.1.3.

lating and characterizing viruses in which the PS was either disrupted (the silPS mutant) or totally ablated (the ΔPS mutant). Three main conclusions can be drawn from the present study. First, the PS ensures the selective inclusion of gRNA over sgRNA in virions, but it is not an absolute prerequisite for gRNA packaging or for particle assembly. The silPS and ΔPS viruses each exhibited a complete loss of packaging selectivity. Purified virions from both mutants contained large quantities of sgRNAs, in contrast to wild-type virions, which overwhelmingly packaged gRNA (Fig. 5E and 7B). However, contrary to our original assumptions, the PS mutants were fully viable and exhibited little or no differences with respect to the wild type in plaque size, plaque morphology, virus titers, or growth kinetics. Moreover, side-by-side preparation and analysis of silPS and wild-type virions revealed that they had essentially the same particle-to-PFU ratio (Fig. 5A).

A second conclusion from our work is that the PS is functional if moved to a different genomic locus. The loss of packaging selectivity in the ΔPS mutant was rescued by placement of a copy of the wild-type PS (PS2) downstream of the replicase gene, showing that the PS is able to act at an ectopic site. The size of the PS2 insertion establishes that a segment corresponding to nucleotides 20,238 to 20,405 of MHV gRNA is sufficient to confer packaging functionality. Although this further delimits the boundaries set by other studies (9, 10, 15), the precise extent of the PS remains to be defined. Finally, we were able to demonstrate that, over the course of multiple passages, the PS provides a fitness advantage to the virus (Fig. 8). Even at initial PFU input ratios that were biased 100:1 to their disadvantage, viruses containing the PS outgrew their otherwise identical counterparts that lacked the PS. This suggests that there must have existed strong evolutionary pressure to retain the PS, once it had been acquired by some common ancestor of the lineage A betacoronaviruses.

For some RNA viruses, such as poliovirus (35) and brome mosaic virus (36), packaging is thought to be primarily driven by a close association between capsid proteins and nascent genomes. Such an association can result from cocompartmentalization or, more directly, from a mechanistic coupling between packaging and RNA replication. For other RNA viruses, such as alphaviruses (37) and retroviruses (38), distinct genomic RNA sequences or structures have been found to play determining roles in the packaging process. Our results indicate that, for MHV, both gRNA and sgRNAs have a propensity for being incorporated into assembling virions. This may be a consequence of their mutual localization in the double-membrane vesicle compartments that are set up by the viral replicase-transcriptase complex (39). Alternatively, there may exist elements other than the PS, common to all viral RNAs, that contribute to the recognition process. The role of the PS appears to be to tilt the balance in the competition between gRNA and the stoichiometrically much more numerous sgRNAs.

Perhaps the closest parallel with our findings can be found in the recently discovered PS of Venezuelan equine encephalitis virus (VEEV) and related alphaviruses (37). VEEV packaging discrim-

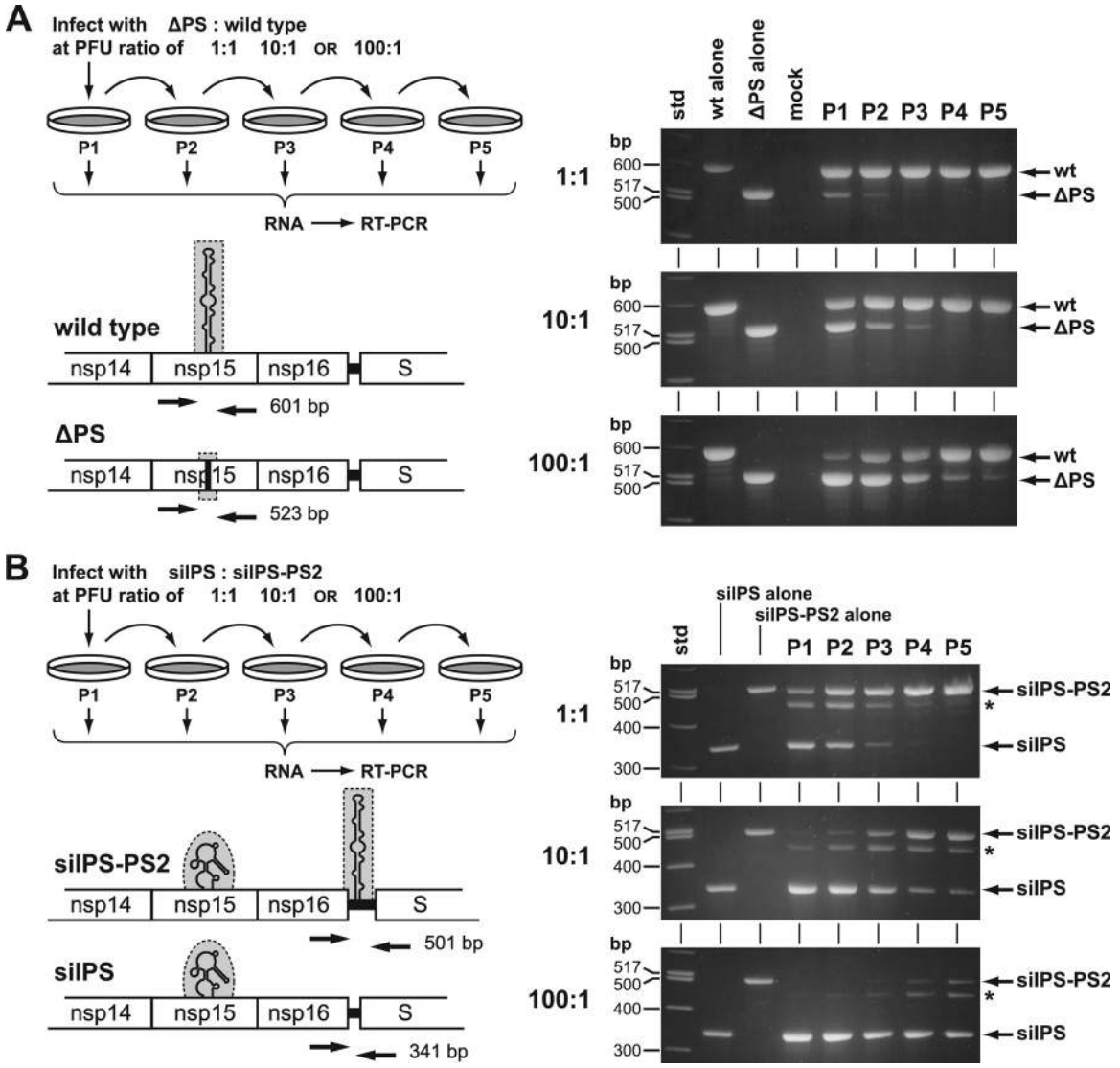

FIG 8 Relative fitness of PS mutants. (A) Monolayers of 17Cl1 cells were coinfected with ΔPS and wild-type viruses at an initial input PFU ratio of 1:1, 10:1, or 100:1, as detailed in Materials and Methods. Harvested released virus was serially propagated for a total of five passages. At each passage, RNA was isolated from infected cells and analyzed by RT-PCR, using a pair of primers flanking the central region of the nsp15 ORF to assay the presence or absence of the PS. PCR products were analyzed by agarose gel electrophoresis; the sizes of DNA markers are indicated on the left of each gel. Control lanes show RT-PCR products obtained from infections with wild-type virus or the ΔPS mutant alone or from uninfected cells (mock). (B) Competition between silPS and silPS-PS2 viruses was evaluated by the same procedure, except that RT-PCR was carried out with a pair of primers flanking the intergenic region between the replicase and the S ORFs to assay the presence or absence of the transposed PS element (PS2). The asterisk to the right of each agarose gel marks the position of an artifactual heteroduplex band formed by opposite strands of the 501-bp silPS-PS2 product and the 341-bp silPS product. The positions and sizes of PCR primers in the schematics are not to scale.

inates between gRNA and a single, abundantly transcribed sgRNA. This is accomplished through recognition of a PS that has been mapped to the nsP1 gene, which is unique to gRNA. Like the MHV PS, the VEEV PS contains a single-stranded purine repeat, in this case a GGG motif displayed in the loops of four to six adjacent hairpin structures. Also, similar to the MHV PS, the VEEV PS retained its function when transposed to a different genomic site. Coding-silent mutational disruption of the VEEV PS caused a high level of packaging of sgRNA. However, unlike the MHV PS mutants, VEEV PS mutants exhibited more severe defects in viral growth kinetics and 30- to 100-fold drops in peak infectious titers compared to the wild type. This more drastic phenotype may result from a limitation on the amount of RNA that can be packaged into the icosahedral alphavirus capsid. In contrast, and highly unusually for positive-strand RNA viruses, coronaviruses have helically symmetric nucleocapsids and pleomorphic envelopes that are likely more able to accommodate additional RNA.

Our demonstration of the principal, and possibly exclusive, role of the MHV PS in the selection of gRNA for virion assembly raises a number of further issues. One of the most immediate questions is the identity of the interacting partner that carries out the selection of gRNA. The obvious candidate for this activity is the nucleocapsid (N) protein, which is the only known protein

constituent of the viral nucleocapsid. Indeed, specific binding of N protein to the PS has been detected *in vitro* by gel shift and UV cross-linking assays (9). On the other hand, a study with MHV virus-like particles found that the principle component of the virion envelope, the membrane (M) protein, was responsible for the selective packaging of nonviral RNA containing the PS, and this packaging occurred in the absence of N protein (40). We hope to use genetic approaches to clarify these apparently contradictory results. Another significant question arising from the role of the MHV PS is how packaging selectivity is determined in coronaviruses that fall outside betacoronavirus lineage A. It can readily be seen that the region of the nsp15 ORF that contains the MHV PS is absent from most other coronaviruses (Fig. 6B). Dissection of packaged DI RNAs has shown that the PS of the alphacoronavirus TGEV is confined to the 5′-most 649 nucleotides of the genome of that virus (6). Similarly, the composition of a packaged DI RNA of the gammacoronavirus IBV rules out almost all of the nsp15 ORF as a potential locus for the PS of that virus (21). Thus, the PSs of different groups of coronaviruses have evolved at different genomic locations, in a manner analogous to the disperse positioning of *cre* elements in picornavirus genomes (41, 42). Our MHV PS mutants, if combined with the appropriate selective factor(s), may provide an opportunity to identify heterologous PS elements. Specifically, we would like to be able to test the prediction that some PSs encompass particular repeated loop motifs found in the 5′ UTRs of various alpha- and betacoronavirus genomes (20). Such future work will potentially reveal unifying principles governing coronavirus gRNA packaging.

ACKNOWLEDGMENTS

We are grateful to Joachim Jaeger for providing the PyMol figure of MHV nsp15. We thank the Applied Genomics Technology Core Facility of the Wadsworth Center for DNA sequencing.

This work was supported by National Institutes of Health (National Institute of Allergy and Infectious Diseases) grants R01 AI064603 and R56 AI064603.

REFERENCES

1. **Masters PS.** 2006. The molecular biology of coronaviruses. Adv. Virus Res. **66**:193–292.
2. **Perlman S, Netland J.** 2009. Coronaviruses post-SARS: update on replication and pathogenesis. Nat. Rev. Microbiol. **7**:439–450.
3. **Makino S, Yokomori K, Lai MMC.** 1990. Analysis of efficiently packaged defective interfering RNAs of murine coronavirus: localization of a possible RNA-packaging signal. J. Virol. **64**:6045–6053.
4. **van der Most RG, Bredenbeek PJ, Spaan WJM.** 1991. A domain at the 3′ end of the polymerase gene is essential for encapsidation of coronavirus defective interfering RNAs. J. Virol. **65**:3219–3226.
5. **Fosmire JA, Hwang K, Makino S.** 1992. Identification and characterization of a coronavirus packaging signal. J. Virol. **66**:3522–3530.
6. **Escors D, Izeta A, Capiscol C, Enjuanes L.** 2003. Transmissible gastroenteritis coronavirus packaging signal is located at the 5′ end of the virus genome. J. Virol. **77**:7890–7902.
7. **Hofmann MA, Sethna PB, Brian DA.** 1990. Bovine coronavirus mRNA replication continues throughout persistent infection in cell culture. J. Virol. **64**:4108–4114.
8. **Zhao X, Shaw K, Cavanagh D.** 1993. Presence of subgenomic mRNAs in virions of coronavirus IBV. Virology **196**:172–178.
9. **Molenkamp R, Spaan WJM.** 1997. Identification of a specific interaction between the coronavirus mouse hepatitis virus A59 nucleocapsid protein and packaging signal. Virology **239**:78–86.
10. **Narayanan K, Makino S.** 2001. Cooperation of an RNA packaging signal and a viral envelope protein in coronavirus RNA packaging. J. Virol. **75**:9059–9067.
11. **Ivanov KA, Hertzig T, Rozanov M, Bayer S, Thiel V, Gorbalenya AE, Ziebuhr J.** 2004. Major genetic marker of nidoviruses encodes a replicative endoribonuclease. Proc. Natl. Acad. Sci. U. S. A. **101**:12694–12699.
12. **Ricagno S, Egloff MP, Ulferts R, Coutard B, Nurizzo D, Campanacci V, Cambillau C, Ziebuhr J, Canard B.** 2006. Crystal structure and mechanistic determinants of SARS coronavirus nonstructural protein 15 define an endoribonuclease family. Proc. Natl. Acad. Sci. U. S. A. **103**:11892–11897.
13. **Kang H, Bhardwaj K, Li Y, Palaninathan S, Sacchettini J, Guarino L, Leibowitz JL, Kao CC.** 2007. Biochemical and genetic analyses of murine hepatitis virus nsp15 endoribonuclease. J. Virol. **81**:13587–13597.
14. **Woo K, Joo M, Narayanan K, Kim KH, Makino S.** 1997. Murine coronavirus packaging signal confers packaging to nonviral RNA. J. Virol. **71**:824–827.
15. **Cologna R, Hogue BG.** 2000. Identification of a bovine coronavirus packaging signal. J. Virol. **74**:580–583.
16. **Bos ECW, Dobbe JC, Luytjes W, Spaan WJM.** 1997. A subgenomic mRNA transcript of the coronavirus mouse hepatitis virus strain A59 defective interfering (DI) RNA is packaged when it contains the DI packaging signal. J. Virol. **71**:5684–5687.
17. **Chen SC, van den Born E, van den Worm SH, Pleij CW, Snijder EJ, Olsthoorn RC.** 2007. New structure model for the packaging signal in the genome of group IIa coronaviruses. J. Virol. **81**:6771–6774.
18. **Carstens EB.** 2010. Ratification vote on taxonomic proposals to the International Committee on Taxonomy of Viruses. Arch. Virol. **155**:133–146.
19. **Joseph JS, Saikatendu KS, Subramanian V, Neuman BW, Buchmeier MJ, Stevens RC, Kuhn P.** 2007. Crystal structure of a monomeric form of severe acute respiratory syndrome coronavirus endonuclease nsp15 suggests a role for hexamerization as an allosteric switch. J. Virol. **81**:6700–6708.
20. **Chen SC, Olsthoorn RC.** 2010. Group-specific structural features of the 5′-proximal sequences of coronavirus genomic RNAs. Virology **401**:29–41.
21. **Penzes Z, Tibbles K, Shaw K, Britton P, Brown TDK, Cavanagh D.** 1994. Characterization of a replicating and packaged defective RNA of avian coronavirus infectious bronchitis virus. Virology **203**:286–293.
22. **Goebel SJ, Hsue B, Dombrowski TF, Masters PS.** 2004. Characterization of the RNA components of a putative molecular switch in the 3′ untranslated region of the murine coronavirus genome. J. Virol. **78**:669–682.
23. **Kuo L, Godeke GJ, Raamsman MJ, Masters PS, Rottier PJ.** 2000. Retargeting of coronavirus by substitution of the spike glycoprotein ectodomain: crossing the host cell species barrier. J. Virol. **74**:1393–1406.
24. **Kuo L, Masters PS.** 2010. Evolved variants of the membrane protein can partially replace the envelope protein in murine coronavirus assembly. J. Virol. **84**:12872–12885.
25. **Ye R, Montalto-Morrison C, Masters PS.** 2004. Genetic analysis of determinants for spike glycoprotein assembly into murine coronavirus virions: distinct roles for charge-rich and cysteine-rich regions of the endodomain. J. Virol. **78**:9904–9917.
26. **Hurst KR, Koetzner CA, Masters PS.** 2009. Identification of in vivo-interacting domains of the murine coronavirus nucleocapsid protein. J. Virol. **83**:7221–7234.
27. **Züst R, Miller TB, Goebel SJ, Thiel V, Masters PS.** 2008. Genetic interactions between an essential 3′ cis-acting RNA pseudoknot, replicase gene products, and the extreme 3′ end of the mouse coronavirus genome. J. Virol. **82**:1214–1228.
28. **Nakamura Y, Gojobori T, Ikemura T.** 2000. Codon usage tabulated from international DNA sequence databases: status for the year 2000. Nucleic Acids Res. **28**:292.
29. **Zuker M.** 2003. Mfold web server for nucleic acid folding and hybridization prediction. Nucleic Acids Res. **31**:3406–3415.
30. **de Haan CA, Masters PS, Shen X, Weiss S, Rottier PJ.** 2002. The group-specific murine coronavirus genes are not essential, but their deletion, by reverse genetics, is attenuating in the natural host. Virology **296**:177–189.
31. **Koetzner CA, Kuo L, Goebel SJ, Dean AB, Parker MM, Masters PS.** 2010. Accessory protein 5a is a major antagonist of the antiviral action of interferon against murine coronavirus. J. Virol. **84**:8262–8274.
32. **Zhao L, Jha BK, Wu A, Elliott R, Ziebuhr J, Gorbalenya AE, Silverman RH, Weiss SR.** 2012. Antagonism of the interferon-induced OAS-RNase L pathway by murine coronavirus ns2 protein is required for virus replication and liver pathology. Cell Host Microbe **11**:607–616.
33. **Xu X, Zhai Y, Sun F, Lou Z, Su D, Xu Y, Zhang R, Joachimiak A, Zhang XC, Bartlam M, Rao Z.** 2006. New antiviral target revealed by the hexa-

meric structure of mouse hepatitis virus nonstructural protein nsp15. J. Virol. **80**:7909–7917.
34. **Bhardwaj K, Liu P, Leibowitz JL, Kao CC.** 2012. The coronavirus endoribonuclease nsp15 interacts with retinoblastoma tumor suppressor protein. J. Virol. **86**:4294–4304.
35. **Nugent CI, Johnson KL, Sarnow P, Kirkegaard K.** 1999. Functional coupling between replication and packaging of poliovirus replicon RNA. J. Virol. **73**:427–435.
36. **Annamalai P, Rao ALN.** 2006. Packaging of brome mosaic virus subgenomic RNA is functionally coupled to replication-dependent transcription and translation of coat protein. J. Virol. **80**:10096–10108.
37. **Kim DY, Firth AE, Atasheva S, Frolova EI, Frolov I.** 2011. Conservation of a packaging signal and the viral genome RNA packaging mechanism in alphavirus evolution. J. Virol. **85**:8022–8036.
38. **D'Souza V, Summers MF.** 2005. How retroviruses select their genomes. Nat. Rev. Microbiol. **3**:643–655.
39. **Knoops K, Kikkert M, Worm SH, Zevenhoven-Dobbe JC, van der Meer Y, Koster AJ, Mommaas AM, Snijder EJ.** 2008. SARS-coronavirus replication is supported by a reticulovesicular network of modified endoplasmic reticulum. PLoS Biol. **6**:e226. doi:10.1371/journal.pbio.0060226.
40. **Narayanan K, Chen CJ, Maeda J, Makino S.** 2003. Nucleocapsid-independent specific viral RNA packaging via viral envelope protein and viral RNA signal. J. Virol. **77**:2922–2927.
41. **Cordey S, Gerlach D, Junier T, Zdobnov EM, Kaiser L, Tapparel C.** 2008. The cis-acting replication elements define human enterovirus and rhinovirus species. RNA **14**:1568–1578.
42. **Steil BP, Barton DJ.** 2009. Cis-active RNA elements (CREs) and picornavirus RNA replication. Virus Res. **139**:240–252.